Am J Transl Res 2019;11(1):142-159
www.ajtr.org /ISSN:1943-8141/AJTR0079125

*Original Article*

# Osthole protects against Ang II-induced endotheliocyte death by targeting NF-κB pathway and Keap-1/Nrf2 pathway

Luyuan Tao, Xingjian Gu, Enguo Xu, Shijia Ren, Li Zhang, Wenhua Liu, Xiaofeng Lin, Jianguang Yang, Changgong Chen

*Department of Cardiology, Taizhou First People's Hospital, Taizhou 318020, Zhejiang, P. R. China*

Received May 6, 2018; Accepted October 27, 2018; Epub January 15, 2019; Published January 30, 2019

**Abstract:** Osthole, the main active constituents in traditional Chinese medicine fructus cnidii, has anti-inflammatory and anti-oxidant activities. Apoptosis of vascular endothelial cells is an important cause of cardiovascular disease. Inflammation and oxidative stress are two key factors in injury of endotheliocyte. In this study, we investigated the effect of osthole on Ang II-induced apoptosis of rat aortic endothelial cells (RAECs) and explored the underlying mechanisms. In the present study, the protective effects of osthole on RAECs induced by Ang II in vitro were tested. Additionally, molecular docking and molecular dynamics (MD) simulations were utilized to investigate the potential binding mode of osthole to NF-κB and Keap1. Our results showed osthole remarkably attenuates Ang II-induced apoptosis of RAECs via alleviating inflammation and oxidative stress. Molecular docking and MD simulations revealed the potential interaction of osthole bind to the P65 subunit of NF-κB and the Keap1 protein, an adaptor for the degradation of Nrf2. We further found that osthole decreased Ang II-induced inflammation and oxidative stress through respectively modulating NF-κB and Nrf2 pathways in RAECs. These studies provide evidence that osthole may represent a potential therapeutic agent for the treatment of vascular injury.

**Keywords:** Osthole, Ang II, inflammation, oxidative stress, rat aortic endothelial cells

## Introduction

High blood pressure (BP), or hypertension, is the leading risk factor for global disease burden [1]. Hypertension is associated with vascular injury that results in increased vascular resistance, which contributes to further development of hypertension and end organ damage [2]. It is well known that is associated with elevated circulating angiotensin II (Ang II) which has an important role in the biological process leading to vascular injury [3, 4]. In addition to its physiological role in arterial blood pressure regulation (ie, via vasoconstriction and retention of sodium and water), Ang II directly induces vascular injury through activating inflammation and oxidative stress [5]. Many studies support the observation that Ang II has direct effects on vascular endothelial cells, including inflammation, hypertrophy, fibrosis, apoptosis, and accumulation of extracellular matrix [4-7]. Thus, an agent targeting Ang II-induced vascular injury may provide a new strategy for the treatment of vascular diseases.

Ang II can increase the expression of pro-inflammatory cytokines and induce cellular oxidative stress. It has been shown in vivo and in vitro that Ang II can activate the canonical pro-inflammatory nuclear factor-κB (NF-κB) pathway [8, 9]. Acute increases in plasma Ang II levels activated NF-κB in endothelial cells [10], therefore increasing expression of several pro-inflammatory cytokines including interleukins (IL) 1-β and -6 in the mouse's abdominal aorta as well as an increase recruitment of monocyte [11]. Ang II-induced apoptosis has been well demonstrated in a number of culture studies [12-14]. These studies have also reported that increased Ang II may be active in the cellular oxidation-reduction reactions resulting in the formation of excess free radicals [12, 13]. The concept that emerges from these observations is that elevated plasma Ang II levels, either as a

result of hypertension, can produce a combined state of low grade inflammation and oxidative stress in various organs including the vascular, which leading to cell apoptosis [14]. The potential roles of inflammation and oxidative stress in cardiovascular disorders suggest that molecules with anti-inflammatory and antioxidant properties may enhance the efficacy of treatment protocols designed to mitigate Ang II-induced injury.

Osthole (also known as osthol), is a natural coumarin first derived from Cnidium plant. High content of osthole is found in the mature fruit of Cnidium monnieri (Fructus Cnidii), which is commonly applied in clinical practice of Traditional Chinese Medicine (TCM) [15]. It has several pharmacological and biological properties such as being an antioxidant, anticancer, anti-inflammatory, antimicrobial, hepatoprotective and immunomodulatory agent [16-18]. Plenty of studies revealed that osthole exerts a powerful reactive oxygen species scavenging effect with potent anti-inflammatory effects [19]. Its anti-inflammatory activity is mediated through multiple mechanisms involving inhibition of various transcription factors such as NF-κB/MAPK pathway and down-regulation of pro-inflammatory cytokines such as TNF-α and IL-6 [20, 21]. In addition, accumulating experimental evidences have shown osthole up-regulate the expression and activity of nuclear factor erythroid 2 (Nrf2), whose downstream proteins were shown to have important protective functions against oxidative stress [22]. Osthole also has vasorelaxant properties and cardiovascular benefits [15]. However, the effect of osthole on Ang II-stimulated apoptosis of endothelial cells is unclear and the direct target of osthole is still unknown.

In the present study, we explored the effect and mechanism of osthole against Ang II-stimulated endothelial cells and further utilizing molecular docking technology investigated the anti-inflammatory and antioxidant target of osthole. Our results demonstrated that osthole can attenuate Ang II-induced endothelial cells by reducing inflammation and ROS in rat aortic endothelial cells. The beneficial actions of osthole are closely associated with its ability to increase Nrf2 expression and inhibit NF-κB activation.

## Material and methods

### *Chemicals*

Osthole (Ost) was purchased from Sigma-Aldrich (St. Louis, MO). Before used to the biological experiments, compounds were purified by re-crystallization or silica gel chromatography to reach the purity higher than 97.0%. Compound was dissolved in DMSO for in vitro experiments.

### *Cell culture*

Rat aortic endothelial cells (RAECs) were derived from male Sprague-Dawley rat (180-200 g, Wenzhou Medical University, China) aortic endothelium. RAECs were isolated as described earlier [23]. In brief, segments of thoracic aortae (18-24 mm) were excised and immediately put in cold Hanks' Balanced Salt Solution (HBSS). The blood residues in the lumen of the vessels were flushed with HBSS. 1 mg/ml collagenase (Sigma) was used to fill the lumen of vessels and incubated in HBSS at 37°C for 20 min. The effluent from the lumen of vessels was collected and centrifuged at 2800 rpm for 5 min. The pellet was washed and suspended in EGM-2 with 2% fetal bovine serum (FBS) at 37°C in a 95% air/5% $CO_2$ incubator. Experiments were performed on cells at passages 5-8. All dishes were coated with 3% Collagen Type I (BD Biosciences) during the RAECs cultures.

### *MTT assay*

After treatments with Ost (10 μM) or Ang II (1 μM) for 24 h, cells were washed for three times, changed medium into 1 mg/mL MTT solution (100 μL/well, Sigma), and then incubated at 37°C for 4 h. Cell viability was determined by measuring the absorbance by a microplate reader (BioTek SYNERGYTM 4, USA) at 570 nm.

### *Western blot analysis*

RAECs pretreated with osthole (10 μM) for 1 h were incubated with Ang II (1 μM) for 30 mins, 1 h, 8 h or 24 h. Cells were lysated and fifty micrograms of lysates were separated by 10% SDS-PAGE and electrotransferred to a PVDF membrane. Each membrane was preincubated for 1.5 h at room temperature in Tris-buffered saline, pH 7.6, containing 0.05% Tween 20 and

**Table 1.** Primers used for real-time qPCR assay

| Gene | Species | Primers (FW) | Primers (RW) |
|---|---|---|---|
| Bax | Rat | TGAAGACAGGGGCCTTTTTG | AATTCGCCGGAGACACTCG |
| Bcl-2 | Rat | ATGCCTTTGTGGAACTATATGGC | GGTATGCACCCAGAGTGATGC |
| TNF-α | Rat | TACTCCCAGGTTCTCTTCAAGG | GGAGGCTGACTTTCTCCTGGTA |
| IL-6 | Rat | GAGTTGTGCAATGGCAATTC | ACTCCAGAAGACCAGAGCAG |
| ICAM-1 | Rat | AGATCATACGGGTTTGGGCTTC | TATGACTCGTGAAAGAAATCAGCTC |
| VCAM-1 | Rat | TTTGCAAGAAAAGCCAACATGAAAG | TCTCCAACAGTTCAGACGTTAGC |
| β-actin | Rat | AAGTCCCTCACCCTCCCAAAAG | AAGCAATGCTGTCACCTTCCC |
| MCP-1 | Rat | GTCACCAAGCTCAAGAGAGAGA | GAGTGGATGCATTAGCTTCAGA |
| IL-1β | Rat | CACCTCTCAAGCAGAGCACAG | GGGTTCCATGGTGAAGTCAAC |
| Nrf2 | Rat | ACTGTCCCCAGCCCAGAGGC | CCAGGCGGTGGGTCTCCGTA |
| HO-1 | Rat | TCTATCGTGCTCGCATGAAC | CAGCTCCTCAAACAGCTCAA |
| NQO-1 | Rat | ACTACGATCCGCCCCCAACTTCTG | CTTCGGCTCCCCTGTGATGTCGT |

5% non-fat milk. Each PVDF membrane was incubated with specific antibodies. Immunoreactive bands were then detected by incubating with a secondary antibody conjugated with horseradish peroxidase and visualizing using enhanced chemiluminescence reagents (Bio-Rad, Hercules, CA). The amounts of the proteins were analyzed using Image J analysis software version 1.38e and normalized to their respective control. Antibodies for Bax, Bcl-2, cleaved caspase 3, NF-κB P65, lamin B p-IκB-α IκBα, GAPDH, Nrf2, HO-1, and NQO-1. the secondary horseradish peroxidase-conjugated antibody were obtained from Santa Cruz Technology (Santa Cruz, CA). In all western bolt analysis, GAPDH was used as a loading control protein. Figure S1 shows original western images for relevant western blots.

*Real-time quantitative qPCR*

RAECs pretreated with osthole (10 μM) for 1 h were incubated with Ang II (1 μM) for 6 h, then the cells were collected. Total RNA was isolated from cells using TRIZOL (Invitrogen, Carlsbad, CA) according to the manufacturer's instructions. Reverse transcription and quantitative PCR were performed using M-MLV Platinum RT-qPCR Kit (Invitrogen, Carlsbad, CA). Real-time qPCR was carried out using the Eppendorf Real plex 4 instruments (Eppendorf, Hamburg, Germany). Primers for genes including Bax, Bcl-2, TNF-α, IL-6, ICAM-1, VACM-1, MCP-1, IL-1β, Nrf2, HO-1, NQO-1 and β-actin were synthesized in Invitrogen (Invitrogen, Shanghai, China). The primer sequences used were shown in **Table 1**. The relative amount of each gene was normalized to the amount of β-actin.

*siRNA-induced gene silencing*

Gene silencing in cells was achieved using specific siRNA sequences. NF-κB or Nrf2 siRNAs were purchased from Gene Pharma Co. LTD. (Shanghai, China). Specific siRNA sequences were 5'-CUGGAUGACAUCUUAAACUTT-3' for Rat NF-κB, and 5'-GGGAGGAGC UAUUAUCCAUTT-3' for Rat Nrf2. Transfection of RAECs cells with siRNA was carried out using LipofectAMINE™ 2000 (Invitrogen, Carlsbad, CA), according to the manufacturer's instruction.

*TUNEL staining*

RAECs pretreated with osthole (10 μM) for 1 h were incubated with Ang II (1 μM) for 24 h and then cells were harvested. Terminal deoxynucleotidyl-transferase-mediated dUTPnick-end labeling (TUNEL) staining was performed on formalin-fixed, paraffinembedded cells with Apoptosis Detection Kit C1086 (Beyotime, China) according to the manufacturer's instruction. Positively stained apoptotic cells were counted in at least five random microscopic fields belonging to each experimental group recorded with Nikon Eclipse E600 microscopy. The percentages of TUNEL positive cells relative to each group were presented. (200 × amplification; Nikon, Japan).

*Measurement of apoptosis by flow cytometry*

RAECs pretreated with osthole (10 μM) for 1 h were incubated with Ang II (1 μM) for 24 h. To determine cell apoptosis, we harvested cells following treatments washed twice with pre-cooled PBS, and suspended in 1 × loading buf-

fer to achieve the concentration 1 × $10^6$ cells per ml. Cells were stained with 5 μl FITC Annexin V and 1 μl PI at room temperature for 15 min in the dark. The apoptosis cell rate was then measured with use of FACS calibur flow cytometry (BD Biosciences, CA).

*Immunofluorescence staining*

RAECs pretreated with osthole (10 μM) for 1 h were incubated with Ang II (1 μM) for 1 h and then cells were harvested. Immunofluorescent detection for NF-κB was carried out by fixing cells in 100% methanol at -20°C for 5 min. After fixation and permeabilization, cells were washed twice with PBS containing 1% bovine serum albumin (BSA), and incubated with anti-p65 antibody (1:200) overnight at 4°C. TRITC-conjugated secondary antibody (1:200) was used for detection. The stained sections were then viewed under the Nikon fluorescence microscope (200 × amplification; Nikon, Japan).

*Determination of IL-6 and TNF-α by enzyme-linked immunosorbent assay (ELISA)*

RAECs pretreated with osthole (10 μM) for 1 h were incubated with Ang II (1 μM) for 24 h. The IL-6 and TNF-α levels in medium of rat aortic endothelial cells were determined with an ELISA kit (Bioscience, San Diego, CA) according to the manufacturer's instructions. The total amount of IL-6 and TNF-α in the cell medium was normalized to the total amount of protein in the viable cell pellets.

*$H_2O_2$ and $O_2^-$ staining*

RAECs pretreated with osthole (10 μM) for 1 h were incubated with Ang II (1 μM) for 12 h. In order to analyze the ROS generation, various subtypes of ROS such as superoxide ($O_2^-$) and hydrogen peroxide ($H_2O_2$) were detected using 5 μM DHE and 2 μM DAF-2DA, respectively, as described previously [13]. The fluorescence intensity for 10,000 events was acquired using FACS, and cellular images were captured under the Nikon fluorescence microscope (200 × amplification; Nikon, Japan).

*Determination of ROS generation by flow cytometry*

RAECs pretreated with osthole (10 μM) for 1 h were incubated with Ang II (1 μM) for 12 h. The cellular hydrogen peroxide ($H_2O_2$) was detected using dichloro dihydro fluorescent (DCF) as described previously [24]. The fluorescence intensity for 10,000 events was acquired using FACS.

*Molecular docking*

To investigate the probable binding mode of osthole to Keap1 and NF-κB as the potential inhibitor, molecular docking was utilized to construct the Keap1/osthole and NF-κB/osthole models by the latest version of AutoDock 4.2.6 package [25]. The crystal structures of Keap1 (PDB entry: 4L7B) and NF-κB (PDB entry: 1NFK) were obtained from Protein Data Bank [26, 27]. Before the docking step, AutoDock4 atomic radii were assigned to the proteins of Keap1 and NF-κB protein. Thereafter, Gasteiger partial charges were assigned to osthole. The binding site of inhibitors for human Keap1 and NF-κB has been well characterized based on previous reported studies [26, 28-30]. The docking protocol were as follows: trials of 200 dockings, population size of 300, maximum number of evaluation 25000000 and other parameters were set as default.

*Molecular dynamics (MD) simulations*

The results from molecular docking were used as the initial structures for the MD simulations. The partial charges of osthole were employ by restrained electrostatic potential (RESP) fitting method based on the electrostatic potentials computed at Hartree-Fock (HF) SCF/6-31G* level of theory [31]. The proteins and osthole were described by the Amber ff14SB force field and generalized Amber force field (GAFF) by LEaP modules in Amber 16 program [32]. Then, each system was immersed in a water box of the TIP3P water mode with at least a 15 Å distance around the complex. Lastly, an appropriate number of counter ions were added to ensure the electro-neutrality for each system. Before the MD productive simulations, an equilibration protocol was performed. Initially, energy minimization was carried out for each system by three steps, including minimization of all the water molecules, side chains of proteins, all the molecules in the water box. In each step, energy minimization was performed by the 2500 steps of steepest descent algorithm and 2500 steps of conjugated gradient algorithm with a non-bonded cutoff of 10 Å. Thereafter, each system was heated to 300 K using at constant volume over a period of 200 ps. Then, each system was equilibrated at constant pres-

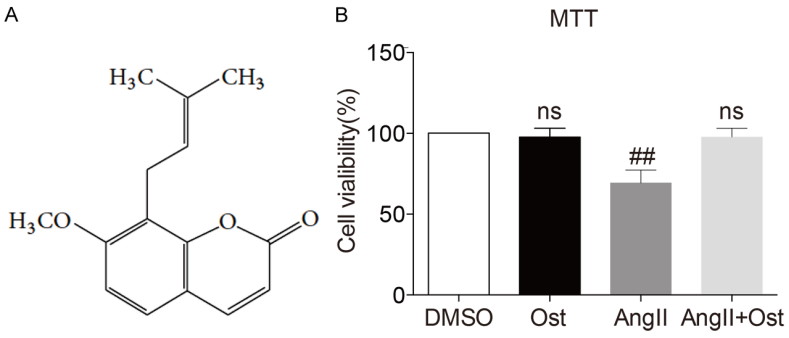


**Figure 1.** The structure of osthole and osthole have no effect on cell viability. A. The structure of osthole. B. Effect of osthole on cell viability was detected by MTT assay as described in the Materials and methods section. (n = 4 independent experiments, ns, no significance vs DMSO).

sure for 1 ns. Ultimately, each system was submitted to 100 ns conventional MD simulation in the NTP ensemble without any restrain. Temperature were maintained using the Langevin temperature scalings [33]. Particle Mesh Ewald (PME) algorithm was utilized to consider the long-range electrostatic interactions of a periodic box with cutoff of 8.0 Å and bond lengths involving hydrogen atoms were constrained by the SHAKE algorithm [34, 35]. A time step of 2 fs was performed and coordinates were saved every 10 ps for further analysis.

*Binding free energy calculations*

MM/GBSA methodology calculate the binding free energy ($\Delta G_{bind}$) by utilizing a thermodynamic cycle that combines the molecular mechanical (MM) energies with the continuum solvent approaches [36]. The $\Delta G_{bind}$ in this study was calculated by using the following equations:

$$\Delta G_{bind} = \Delta G_{comp} - (\Delta G_{rec} + \Delta G_{lig}) \quad (1)$$

$$\Delta G_{bind} = \Delta E_{MM} + \Delta G_{sol} - T\Delta S \quad (2)$$

$$\Delta E_{MM} = \Delta E_{int} + \Delta E_{vdW} + \Delta E_{elec} \quad (3)$$

$$\Delta G_{sol} = \Delta G_{GB} + \Delta G_{SA} \quad (4)$$

Where $\Delta G_{comp}$, $\Delta G_{rec}$, and $\Delta G_{lig}$ are the free energies of receptor-ligand complex, receptor, and ligand, respectively (equation 1). $\Delta E_{MM}$ and $\Delta G_{sol}$ represent the MM interaction energy and solvation energy. $T\Delta S$, represents the change of the conformational entropy upon ligand binding at temperature T. In equation 3, $\Delta E_{MM}$ can be split into three terms: intermolecular interaction energy ($\Delta E_{int}$), van der Waals energy ($\Delta E_{vdW}$), and electrostatic energy ($\Delta E_{elec}$). The $\Delta G_{sol}$ includes the polar ($\Delta G_{GB}$) and nonpolar ($\Delta G_{SA}$) parts (equation 4). In this study, the $\Delta G_{GB}$ was calculated using a Generalized-Boltzmann (GB) model at igb = 2 [37]. Dielectric constants of 80.0 and 1.0 were used for solvent and solute, respectively. The $\Delta G_{SA}$ was estimated by relating it to the solvent accessible surface area (SASA) with coefficient of 0.0072. Trajectories from MD simulations between 80 and 100 ns with 500 snapshots were utilized to binding free energy calculations and free energy decompositions. $T\Delta S$ was not estimated due to the high computational demand and low prediction accuracy [38].

*Statistical analysis*

Each in vitro experiment was performed in a group size of n>3 independent samples. Representative images from 3 independent experiments were shown. Data were presented as means ± SEMs. The statistical significance of differences between groups was obtained by ANOVA multiple comparisons in GraphPad Pro 5.0 (GraphPad, San Diego, CA). Differences were considered to be significant at $P<0.05$.

## Results

*Osthole have no effect on cell viability*

The chemical structure of osthole is shown in **Figure 1A**. We initially determined the effect of osthole on cell viability. RACEs were incubated with 10 μM osthole or Ang II for 24 h, and then proliferation of cell was examined by MTT assay. As **Figure 1B** shown, Ang II induced apoptosis of RAECs, but osthole had no obvious effect on viability of RAECs. Pretreatment of RAECs with osthole (10 μM) significantly decreased apoptotic cells.

*Osthole attenuates Ang II-induced inflammation in RAECs by inhibiting activation of NF-κB signaling pathway*

Endothelial inflammation damage is an important cause of ECs apoptosis in the development and progression of chronic disease [39]. Our

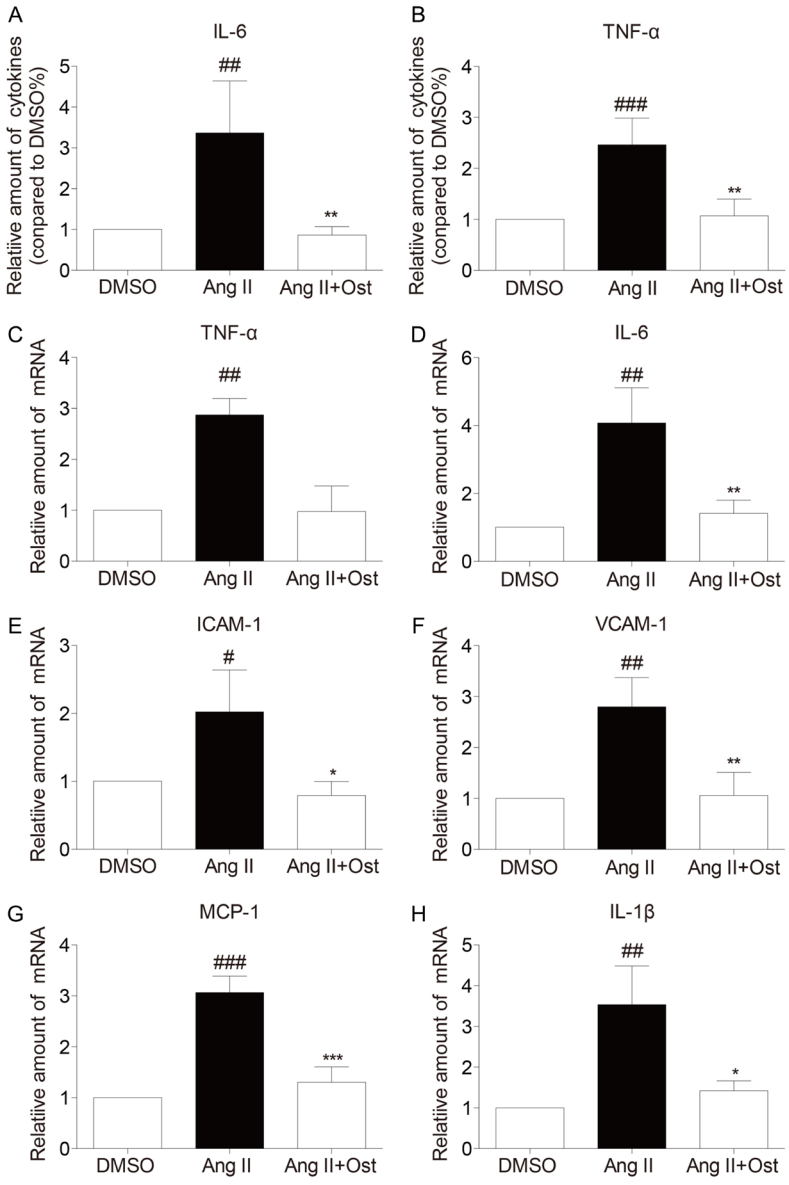


**Figure 2.** Osthole attenuates Ang II-induced inflammation in RAECs. (A, B) Enzyme-linked immunosorbent assay for pro-inflammatory cytokines. The levels of IL-6 (A) and TNF-α (B) in the cultural medium were detected by ELISA. (C-H) mRNA expression of pro-inflammatory cytokines, including TNF-α (C), IL-6 (D), ICAM-1 (E), VCAM-1 (F), MCP-1 (G) and IL-1β (H), were detected by real-time qPCR assay using β-actin as a control gene. (n = 4 independent experiments, $^{\#}P<0.05$, $^{\#\#}P<0.01$, $^{\#\#\#}P<0.001$, vs DMSO; $^{*}P<0.05$, $^{**}P<0.01$, $^{***}P<0.001$, vs Ang II).

next objective was to determine whether osthole exhibits anti-inflammatory activity in Ang II-treated RAECs. Accordingly, we examined whether osthole altered Ang II-induced pro-inflammatory cytokine release. As **Figure 2A**, **2B** showed, Ang II induced the secretion of tumor necrosis factor-α (TNF-α) and interleukin-6 (IL-6) in medium. In addition, real-time qPCR analysis also showed that there were marked increases in the expression of pro-inflammatory genes including TNF-α, IL-6, IL-1β, VCAM-1, ICAM-1 and MCP-1 in RAECs exposed to Ang II (**Figure 2C-H**). Upon treatment with 10 μM osthole, these overproductions were significantly attenuated (**Figure 2A-H**).

It has been found that NF-κB play a critical role in mediating inflammatory response [40]. The degradation of IκB, a key step in the activation of NF-κB signaling pathway, exposes the nuclear localization sequence of NF-κB and enters the nuclear to initiate transcription [41]. Immunofluorescence assay for NF-κB p65 showed that Ang II incubation for 1 h in RAECs remarkably induced translocation of NF-κB p65 subunit from the cytosol to the nucleus (**Figure 3A**, **3B**). Similar results were obtained by western blot (**Figure 3C**). In addition, Incubation with Ang II for 30 min in RAECs significantly induced IκB-α degradation (**Figure 3D**). Nonetheless, these changes were reversed by pretreating with osthole (**Figure 3A-D**).

To further investigate the interaction relationship of osthole and NF-κB, molecular docking and MD simulation were applied. The reported crystal structure of NF-κB consists of two p65 subunits and one DNA molecule connected by a linker. One of p65 subunits was separated from its homo-dimeric for molecular modeling. The root mean square deviations (RMSDs) of the protein backbone atoms and osthole were calculated to monitor the dynamic stability of the initial docked conformation. As shown in **Figure 4A**, the RMSDs of protein were very large during 100 ns MD simulation. On the contrary, the RMSD curves of osthole were relative stable

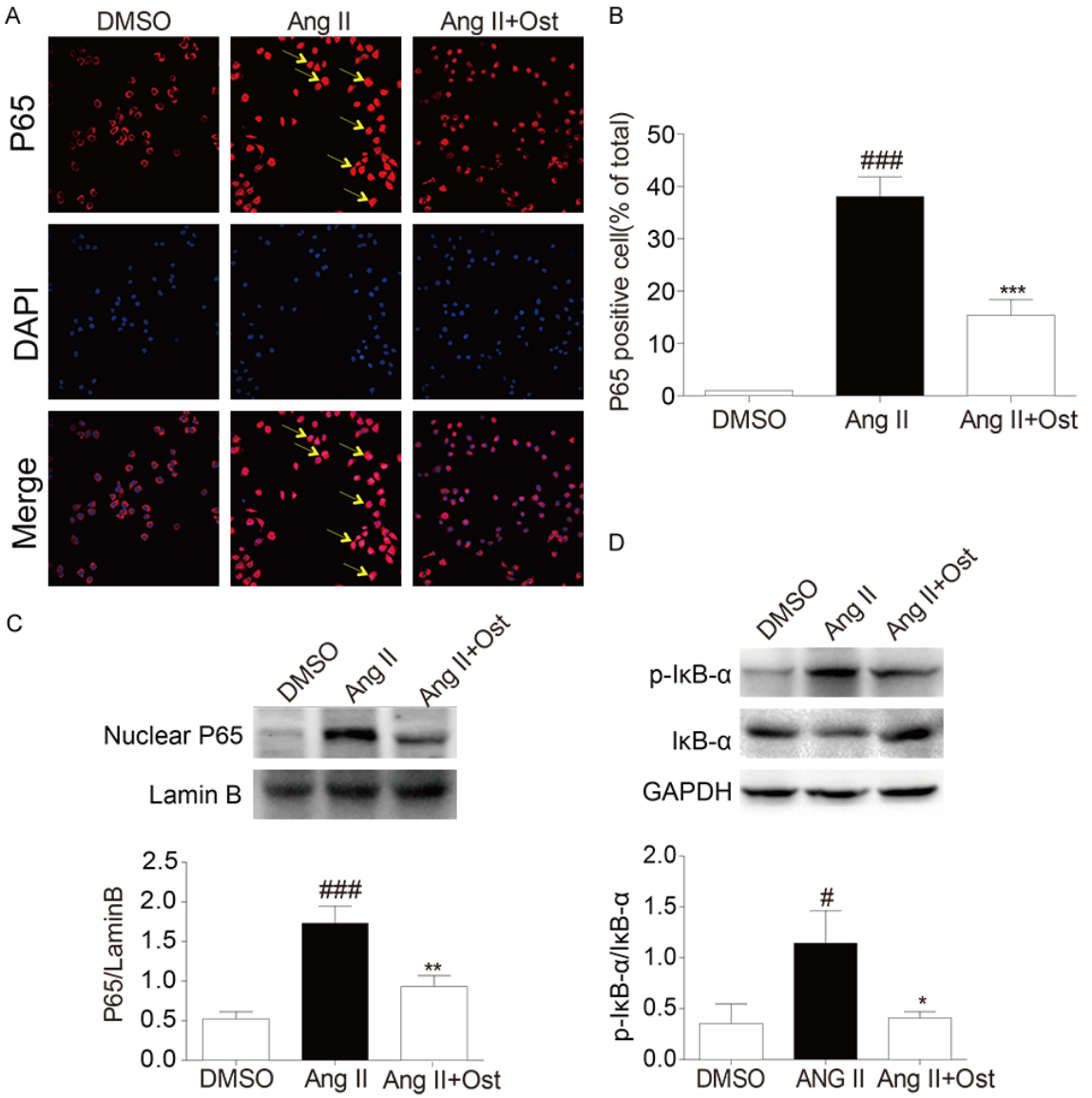


**Figure 3.** Osthole inhibits activation of NF-κB signaling pathway in RAECs. (A, B) Immunofluorescence assay for NF-κB p65 nuclear translocation as described in the Materials and methods section. Representative images for Immunofluorescence were shown (A) with the quantitative column figure for NF-κB p65 nuclear translocation in means ± SE from 3 independent experiments (B) (200 × amplification; Nikon, Japan). (C) Nuclear NF-κB p65 was detected by western blot analysis with Lamin B as a loading control. (D) p-IκB-α, and IκB-α were detected by western blot analysis with GAPDH as a loading control. (n = 4 independent experiments, $^{\#}P<0.05$, $^{\#\#\#}P<0.001$, vs DMSO; $^{*}P<0.05$, $^{**}P<0.01$, $^{***}P<0.001$, vs Ang II).

during the whole simulation. The alignment of starting (yellow) and final (purple) structures showed significantly different. These findings suggested large conformational change occurred when p65 subunit bind to osthole (**Figure 4B**). Furthermore, the energy decomposition was carried out to determine the roles of individual residues in determining protein-ligand interactions. The result showed that the top 5 contributing residues were Gln-128, Gln-132, Ala-129, Val-102, Glu-89 (**Figure 4C**, **4D**). To confirm the anti-inflammation action of osthole is NF-κB-dependent in Ang II-challenged RAECs, we knocked down the expression of NF-κB prior to Ang II exposure. Compared with control group, transfection of cells with specific siRNA reduced protein abundance by more than 70% (**Figure 4E**). Silencing NF-κB down-regulate IL-6 (**Figure 4F**) and TNF-α (**Figure 4G**) secretion in Ang II-induced RAECs, while, osthole was not able to reduce Ang II-induced secretion of IL-6 (**Figure 4F**) and TNF-α (**Figure 4G**) in NF-κB-

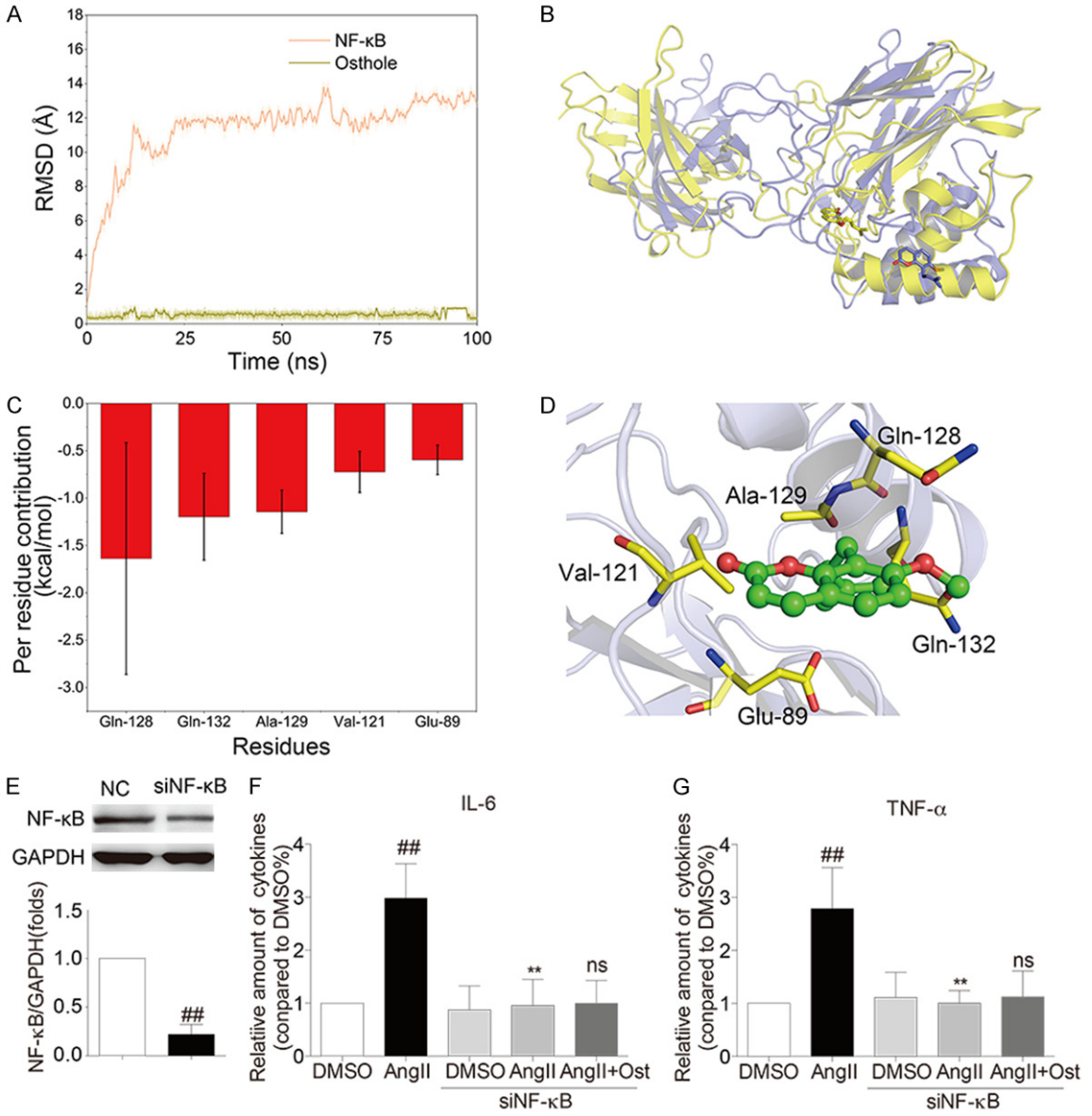


**Figure 4.** Molecular modeling analysis of NF-κB bind to osthole. (A) Time evolution of the RMSD of NF-κB and osthole; (B) The alignments of starting (yellow) and final (purple) structures from MD simulations; (C) Per-residue top 5 contributors to the binding effective energy of osthole in NF-κB; (D) Structure analysis of top 5 contributed residues of osthole in NF-κB. (E) Western blot analysis for silencing NF-κB. (F, G) Enzyme-linked immunosorbent assay for the levels of IL-6 (F) and TNF-α (G) in NF-κB-knockdown RAECs. (n = 4 independent experiments, $^{\#\#}P<0.01$, vs DMSO; $^{**}P<0.01$, vs Ang II; ns, no significance, vs siNF-κB+Ang II).

knockdown RAECs. Overall, these results suggest that osthole attenuates Ang II-induced inflammation in RAECs by inhibiting directly activation of NF-κB signaling pathway.

*Osthole attenuates Ang II-induced oxidative stress in RAECs by activating Nrf2 signaling pathway*

Oxidative stress is considered to be a major ingredient contributing to damage of endothelial cells, and is an important component of the etiology of vascular injury [42]. Signaling pathways regulated by oxidative stress is increasingly recognized as an important contributor to the pathophysiology of vascular injury [43]. We examined the direct effects of osthole on Ang II-induced oxidative stress in RAECs. Evidences from **Figure 5A-D**, Ang II increased the production of $H_2O_2$ (**Figure 5A**, **5B**) and $O_2^-$ (**Figure 5C**, **5D**), which was prevented by osthole in RAECs. Treatment with osthole using a 10 μM concen-

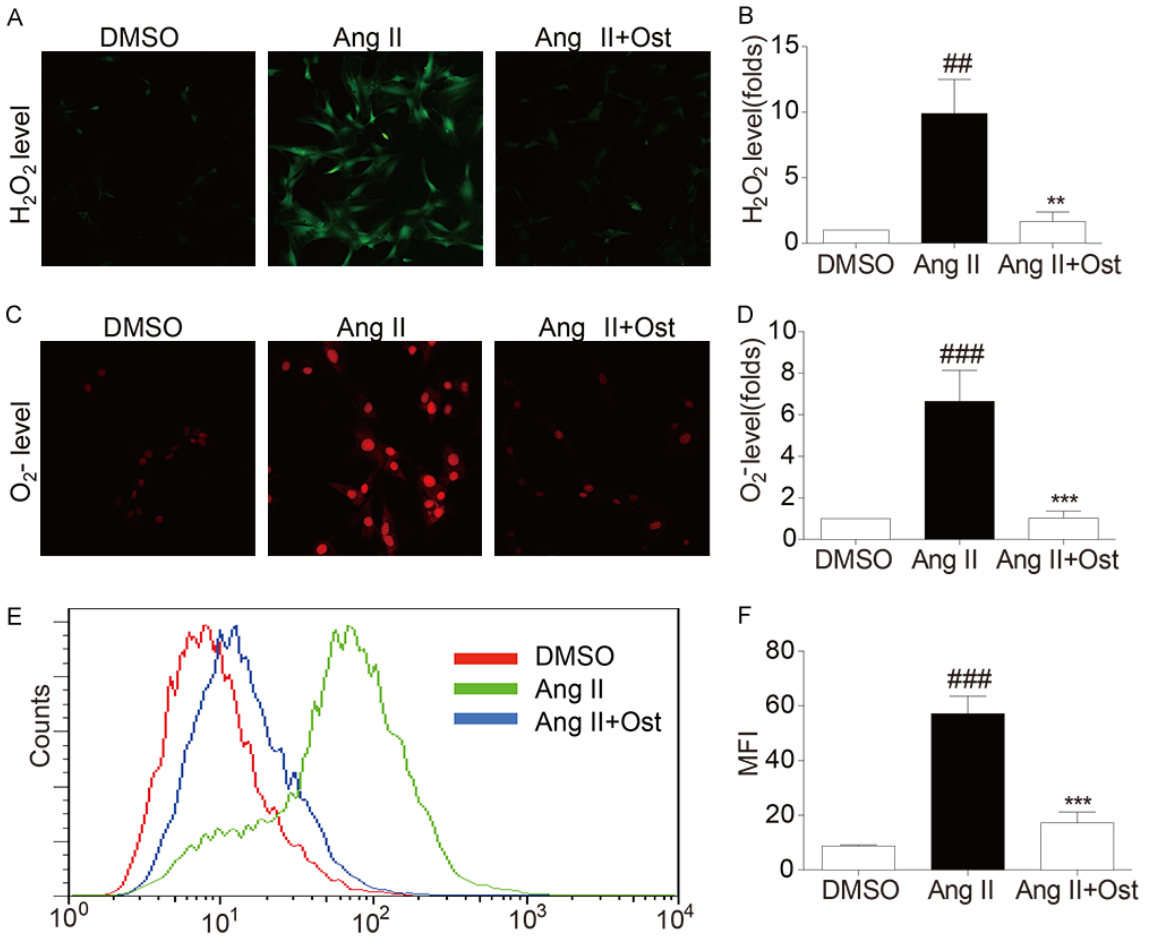


**Figure 5.** Osthole attenuates Ang II-induced oxidative stress in RAECs. (A-D) Representative staining images for $H_2O_2$ (A) and $O_2^-$ (C) levels. The quantitative data in means ± SE from 3 independent experiments (B and D) (200 × amplification; Nikon, Japan). (E, F) Flow cytometry assay for $H_2O_2$ levels. Positive cells were detected using flow cytometry with mean fluorescence intensity (MFI) value of each group (E) and the quantitative data in means ± SE from 3 independent experiments (F). (n = 4 independent experiments, $^{\#\#}P<0.01$, $^{\#\#\#}P<0.001$, vs DMSO; $^{**}P<0.01$, $^{***}P<0.001$, vs Ang II).

tration significantly decreased ROS production with a confirmation using flow cytometry. The mean fluorescent intensity (MFI) values showed that osthole significantly reduced Ang II-induced increases in ROS-positive cells (**Figure 5E**, **5F**). To further investigate the potential mechanism involved in osthole-mediated oxidative stress regulation, we examined Nrf2 signaling pathways. Pretreatment of RAECs with osthole (10 μM) significantly increased Nrf2 expression (**Figure 6A**, **6B**). In consistent with Nrf2 activation, the expression of Nrf2-downstream antioxidant genes including heme oxygenase-1 (HO-1) and NADPH quinine oxidoreductase (NQO-1) were significantly up-regulated in RAECs exposed to Ang II for 12 h by pretreating with osthole (10 μM) (**Figure 6A**, **6C**, **6D**). Similar results were obtained by real-time qPCR analysis (**Figure 6E-G**). In general, Nrf2 is retained unactivated in the cytoplasm by binding with its inhibitor named kelch-like ECH-associated protein-1 (Keap1), which serves as an adaptor for the degradation of Nrf2. Increasing evidences have demonstrated that the Nrf2/Keap1 signaling path way plays important roles in maintaining the balance of cellular redox homeostasis, and has become a vital target for the prevention and treatment of oxidative stress-related diseases. Previous studies indicated that the potential interacting of small molecular inhibitors with Nrf2 binding site in the Keap1 protein [28-30]. To insight into the binding mode of osthole to Keap1, molecular docking and MD simulation were carried out. The RMSDs of the protein backbone atoms and osthole were calculated to investigate the

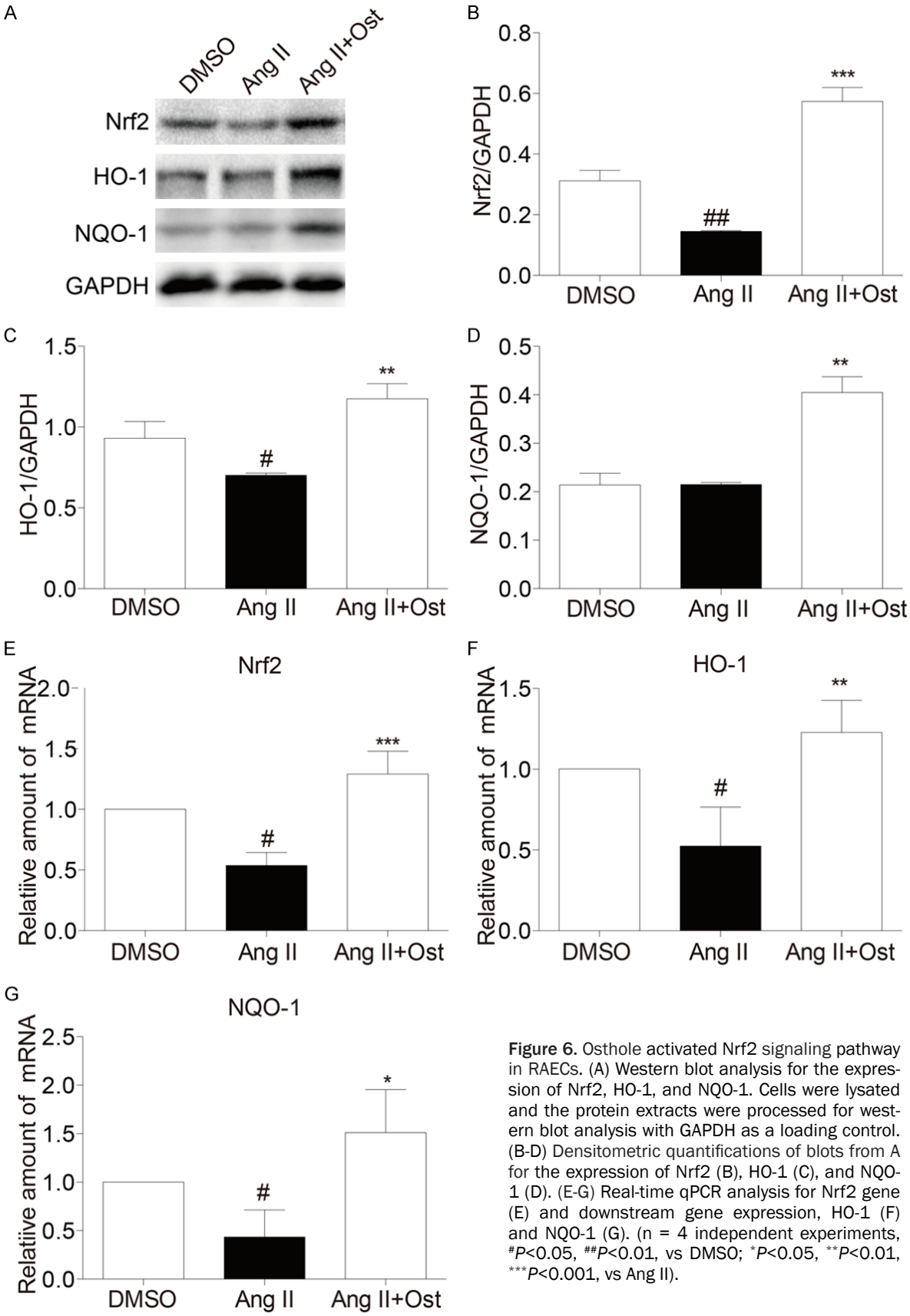


**Figure 6.** Osthole activated Nrf2 signaling pathway in RAECs. (A) Western blot analysis for the expression of Nrf2, HO-1, and NQO-1. Cells were lysated and the protein extracts were processed for western blot analysis with GAPDH as a loading control. (B-D) Densitometric quantifications of blots from A for the expression of Nrf2 (B), HO-1 (C), and NQO-1 (D). (E-G) Real-time qPCR analysis for Nrf2 gene (E) and downstream gene expression, HO-1 (F) and NQO-1 (G). (n = 4 independent experiments, $^{\#}P<0.05$, $^{\#\#}P<0.01$, vs DMSO; $^{*}P<0.05$, $^{**}P<0.01$, $^{***}P<0.001$, vs Ang II).

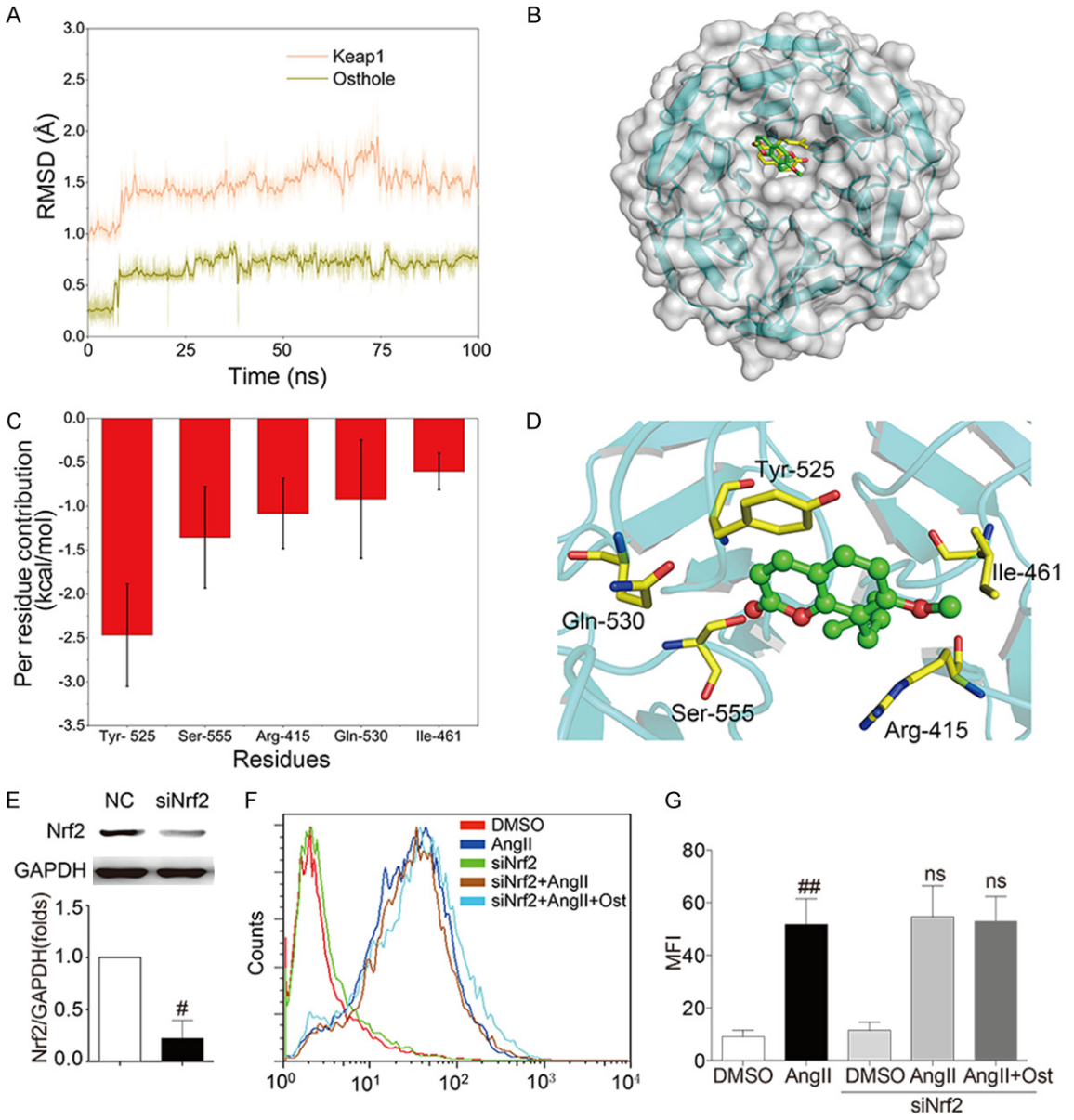


**Figure 7.** Molecular modeling analysis of Keap1 bind to osthole. (A) Time evolution of the RMSD of Keap1 and osthole; (B) The alignments of starting (yellow) and final (green) structures from MD simulations; (C) Per-residue top 5 contributors to the binding effective energy of osthole in Keap1; (D) Structure analysis of top 5 contributed residues of osthole in Keap1. (E) Western blot analysis for silencing Nrf2 (F, G) Flow cytometry assay for $H_2O_2$ levels in Nrf2-knockdown RAECs. Positive cells were detected using flow cytometry with mean fluorescence intensity (MFI) value of each group (F) and the quantitative data (G) in means ± SE from 3 independent experiments. (n = 4 independent experiments, $^{\#\#}P<0.01$, vs DMSO; ns, no significance, vs Ang II).

dynamic stability of the initial docked conformation. As shown in **Figure 7A**, the RMSDs of Keap1 and osthole were quite small during 100 ns MD simulation. The alignment of starting (yellow) and final (purple) structures showed high similarity with appropriate adjustment (**Figure 7B**). It can be concluded that the stable binding of Keap1 to osthole may occupied the portion of the Nrf-2, which was responsible for osthole-mediated oxidative stress regulation (**Figure 7B**). Furthermore, the energy decomposition was applied to determine the roles of individual residues in determining protein-ligand interactions. The result showed that the top 5 contributing residues were Tyr-525, Ser-555, Arg-415, Gln-530, Ile-461 (**Figure 7C**, **7D**).

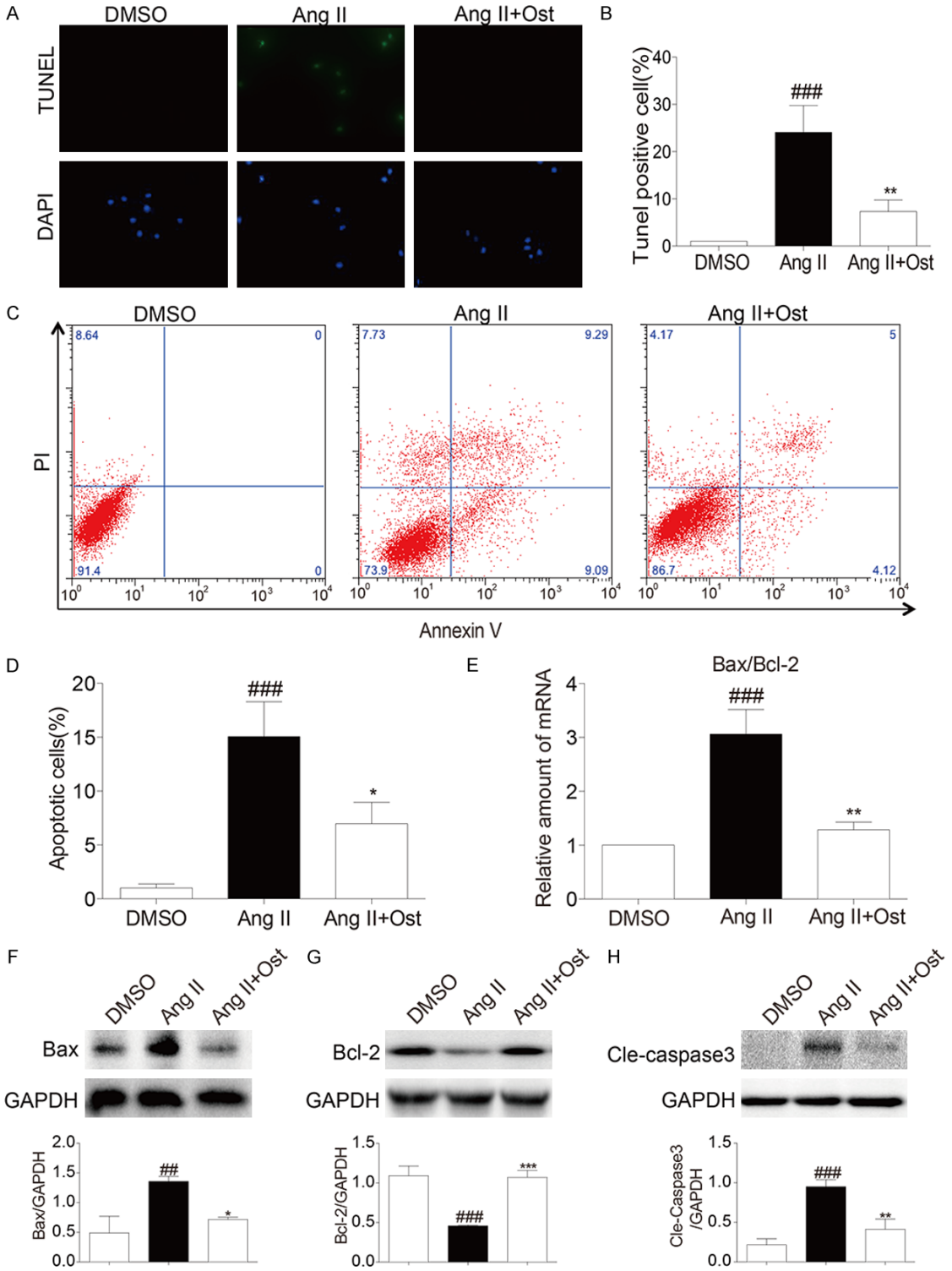


**Figure 8.** Osthole attenuates Ang II-induced apoptosis in RAECs. (A, B) Representative images for TUNEL staining. Representative images for TUNEL staining were shown (A) with the quantitative column figure for TUNEL positive cells in means ± SE from 3 independent experiments (B) (200 × amplification; Nikon, Japan). (C, D) Flow cytometry assay for cell apoptosis. Representative flow cytometry images were shown (C) with the quantitative column figure for apoptotic cells in means ± SE from 3 independent experiments (D). (E) Real-time qPCR assay for mRNA expression for Bax and Bcl-2. (F-H) Western bolt analysis and densitometric quantifications for Bax (F), Bcl-2 (G), and cleaved-casepase 3 (H). The extracted total proteins were processed for western blot analysis with GAPDH as a loading control. (n = 4 independent experiments, $^{\#\#}P<0.01$, $^{\#\#\#}P<0.001$, vs DMSO; $^{*}P<0.05$, $^{**}P<0.01$, $^{***}P<0.001$, vs Ang II).

To confirm the anti-oxidant action of osthole is Nrf2-dependent in Ang II-challenged RAECs, we knocked down the expression of Nrf2 prior to Ang II exposure. Compared with control group, transfection of cells with specific siRNA reduced protein abundance by more than 70% (**Figure 7E**). Compared with control group, silencing Nrf2 has no significant difference in Ang II-induced $H_2O_2$ level of RAECs, while, osthole was not able to reduce Ang II-induced $H_2O_2$ level in Nrf2-knockdown RAECs (**Figure 7F**, **7G**). Consequently, osthole attenuates Ang II-induced oxidative stress in RAECs by activating Nrf2 signaling pathway.

*Osthole attenuates Ang II-induced apoptosis in RAECs*

Ang II-induced damage to endothelial cells (ECs) plays a crucial role in the pathogenesis of vascular disease [44]. ECs apoptosis leads to endothelium dysfunction, which impenetrating in the process of vascular remodeling and injury [45]. We further determined the protective effects of osthole on Ang II-induced RAECs apoptosis. As **Figure 8A**, **8B** shown, Ang II induced RAECs apoptosis after 24 h exposure by TUNEL Staining. We then assayed for annexin V/PI to show that the relative percent of apoptotic cells and the number of annexin V positive cells were significantly higher in Ang II treated cells (**Figure 8C**, **8D**). Treatment with osthole at 10 μM profoundly decreased the number of apoptotic cells as evidenced by TUNEL Staining and flow cytometry (**Figure 8A-D**). Furthermore, Ang II treatment increased the expression of important apoptosis-related protein such as Bax (**Figure 8E**) and cleaved caspase 3 (**Figure 8F**) and decreased the expression of Bcl-2, an anti-apoptotic protein (**Figure 8G**). The ration of Bax/Bcl-2 was also increased after 6 h Ang II treatment (**Figure 8H**). Pretreatment with osthole at 10 μM significantly reversed these changes in apoptosis-related genes induced by Ang II (**Figure 8E-H**). These results show that osthole protected against Ang II-induced RAECs apoptosis.

## Discussion

Hypertension-induced vascular injury assumes a more rapid course, eventually resulting in premature cardiovascular disease, including stroke, myocardial infarction and peripheral artery disease as well as vascular dementia [46]. Hypertension is associated with vascular changes characterized by endothelial dysfunction and vascular remodeling [2]. However, cellular and molecular mechanisms underlying hypertension-associated changes of the vascular system has been unclear. Recent studies have emphasized that oxidative stress and chronic inflammatory processes are important in the pathophysiology of hypertension-related cardiovascular disorder [47]. Uncontrolled production of ROS and inflammatory cytokines induced by Ang II, the major effector in renin-angiotensin-aldosterone system, impairs cellular functions and causes cell apoptosis in a variety of tissues including the blood vessel [47]. Therefore, elucidating the mechanism by which Ang II causes vascular injury and discovering novel therapeutic agents are timely.

Natural products will be helpful in identifying the bioactive lead compounds and develop them into drugs for the treatment of oxidative and inflammatory diseases. Many phytochemicals, especially polyphenolic compounds, possess anti-oxidant and anti-inflammatory bioactivity and have been shown to exhibit protective effect on vascular and circulatory system. Plenty of experimental results have revealed that disease prevention and therapeutics of osthole are associated with its anti-oxidant and anti-inflammatory properties [15]. Recently, Fusi.F and his colleagues showed anti-hypertensive effect of osthole in animal models of hypertension [48]. However, the molecular mechanism of antihypertensive effect of osthole still remains unclear and we devised this study to offer insight in its regulatory functions.

Several reports have shown that hypertension is associated with a state of chronic, low-grade inflammation, suggesting that inflammation may be a potential mechanism whereby hypertension leads to cardiovascular disorder [5]. Ang II elicits many of its (patho) physiological actions by stimulating reactive oxygen species (ROS) generation and inflammatory cytokine expression in cultured aortic smooth muscle cells and endothelial cells [49, 50]. Reports also showed that both circulation Ang II and tissue-based Ang II may affect vascular functions [46, 51]. Recently, a large number of experimental studies have shown that Ang II mediates several key events of the inflammatory processes [52]. In cultured mesangial and vascular smooth muscle, Ang II trigger inflam-

matory responses via increasing expression of toll-like receptor 4, which promotes inflammatory gene expression by triggering NF-κB activation [53]. Among the intracellular signaling system involved in the regulation of inflammatory responses, the transcriptional factor NF-κB has a special position. The upstream IKKα interacts with IκB-α and specifically phosphorylates IκB-α to promote its degradation. The dissociation of IκB-α from the inactive cytoplasmic complex leads to the translocation of the active subunit NF-κB p65 from the cytosolic to nuclear fractions, which binds to certain DNA sites and triggers inflammatory gene expression. Osthole treatment has been associated with a positive outcome in many chronic inflammatory diseases, which exerts anti-inflammatory activity via several mechanisms [15]. For instance, osthole inactivates NF-κB, resulting in the decreased expression of TNF-α, IL-8 and IL-6 in chronic kidney failure (CKF) [54]. Our studies showed that Ang II increase p65 translocation and NF-κB activity in cultured RAECs (**Figure 3A-C**). Osthole significantly inhibited NF-κB activation induced by Ang II thus alleviating the expression of inflammatory cytokines like TNF-α, IL-6, IL-1β, MCP-1, and adhesion molecules (**Figure 2**). Molecular modeling further suggests that osthole can bind to the p65 subunit of NF-κB and trigger the conformational change of p65 subunit, resulting in prevention of the specific DNA binding (**Figure 4A-D**). These findings indicate that osthole inhibits Ang II-induced endothelial inflammation via inactivation of NF-κB.

Ang II has its greatest effect on ROS generation, which may be an important signaling element of hypertension and other delirious action of Ang II [51]. The mechanisms of Ang II-induced ROS actions are not fully understood, yet effective anti-oxidant therapy often attenuates vascular effects of Ang II and hypertension. Here, we observed a significant augmentation of ROS and oxidative stress, when RAECs were exposed to Ang II (**Figure 5**). Many genes involved in oxidative stress response have been shown to regulate Nrf2 directly or indirectly [55]. When activated, Nrf2 is bound to antioxidant transcription elements in the promoter regions of phase 2 detoxification enzyme genes and certain anti-oxidant genes. Nrf2 increases their expression, and leads to cellular resistance to oxidative stress [55]. Li et al. have reported that Nrf2 deficiency exacerbated ROS production in Ang II-induced pathogenesis of cardiac hypertrophy, suggesting that Nrf2 may be a major mediator in Ang II-induced oxidative stress [56]. Interestingly, osthole has an anti-oxidant effect and *in vivo* and *in vitro* studies have indicated its action on triggering Nrf2 signaling, which protect against ROS-mediated damage [19, 22]. However, it is remains unknown whether osthole protects Ang II-induced endothelial injury via Nrf2 activation. Our studies showed that treating with osthole increased the expression of Nrf2 in RAECs (**Figure 6A**, **6B**, **6E**). In addition, we found that the expression of Nrf2-downstream genes HO-1 and NQO-1 are also significantly increased by osthole treatment (**Figure 6A**, **6C**, **6D**, **6F**, **6G**). Our molecular modeling studies further suggest the potential interaction of osthole bind to the P65 subunit of NF-κB and Keap1 protein (**Figure 7**). Overall, these results suggest that osthole-induced Nrf2 activation by prevent the binding of Keap1 and Nrf2 is a possible mechanism against Ang II-induced oxidative stress to attenuate endothelial injury.

It is well known that oxidative stress and inflammation in cells are strongly associated with the induction of apoptosis [57]. An in vitro study revealed that osthole protects PC12 cells against apoptosis through inhibition of ROS production [58]. As a result of oxidative damage and inflammation, we showed that RAECs undergo apoptosis which was evidenced by the enhanced number of apoptotic cells, with increasing expression of Bax and cleaved caspase 3 and the decreased expression of anti-apoptotic protein Bcl-2 (**Figure 8**). These findings prove the anti-apoptosis activity of osthole in Ang II-induced endothelial injury. It is reasonable to speculate osthole reduced apoptosis by alleviating the oxidative stress and inhibiting the NF-κB activation.

Importantly, inflammatory and oxidative stress are closely interrelated in the process of vascular injury. Thus, agents with both anti-oxidant and anti-inflammatory properties may attract more attention for treating the disease. The findings of the present study demonstrate the preventive role of osthole against oxidative stress, inflammation, and apoptosis in Ang II-treated RAECs. The beneficial actions of osthole are closely associated with its ability to inhibit Ang II-induced oxidative stress and

inflammation via activating Nrf2 and inhibiting NF-κB, respectively. Although continued research is needed to examine the underlying molecular target of osthole, this clearly suggests the potential therapeutic application of osthole in the treatment of hypertension-associated disease including vascular injury. In addition, these findings indicated that Nrf2 and NF-κB, regulating the oxidative stress and inflammation respectively, may be important therapeutic targets for hypertension-associated disease.

## Disclosure of conflict of interest

None.

**Address correspondence to:** Changgong Chen, Department of Cardiology, Taizhou First People's Hospital, Hengjie Road, No 218, Huangyan, Taizhou 318020, Zhejiang, P. R. China. E-mail: cgc_tz@126.com

## References

[1] Lim SS, Vos T, Flaxman AD, Danaei G, Shibuya K, Adair-Rohani H, Amann M, Anderson HR, Andrews KG, Aryee M, Atkinson C, Bacchus LJ, Bahalim AN, Balakrishnan K, Balmes J, Barker-Collo S, Baxter A, Bell ML, Blore JD, Blyth F, Bonner C, Borges G, Bourne R, Boussinesq M, Brauer M, Brooks P, Bruce NG, Brunekreef B, Bryan-Hancock C, Bucello C, Buchbinder R, Bull F, Burnett RT, Byers TE, Calabria B, Carapetis J, Carnahan E, Chafe Z, Charlson F, Chen H, Chen JS, Cheng AT, Child JC, Cohen A, Colson KE, Cowie BC, Darby S, Darling S, Davis A, Degenhardt L, Dentener F, Des Jarlais DC, Devries K, Dherani M, Ding EL, Dorsey ER, Driscoll T, Edmond K, Ali SE, Engell RE, Erwin PJ, Fahimi S, Falder G, Farzadfar F, Ferrari A, Finucane MM, Flaxman S, Fowkes FG, Freedman G, Freeman MK, Gakidou E, Ghosh S, Giovannucci E, Gmel G, Graham K, Grainger R, Grant B, Gunnell D, Gutierrez HR, Hall W, Hoek HW, Hogan A, Hosgood HD 3rd, Hoy D, Hu H, Hubbell BJ, Hutchings SJ, Ibeanusi SE, Jacklyn GL, Jasrasaria R, Jonas JB, Kan H, Kanis JA, Kassebaum N, Kawakami N, Khang YH, Khatibzadeh S, Khoo JP, Kok C, Laden F, Lalloo R, Lan Q, Lathlean T, Leasher JL, Leigh J, Li Y, Lin JK, Lipshultz SE, London S, Lozano R, Lu Y, Mak J, Malekzadeh R, Mallinger L, Marcenes W, March L, Marks R, Martin R, McGale P, McGrath J, Mehta S, Mensah GA, Merriman TR, Micha R, Michaud C, Mishra V, Mohd Hanafiah K, Mokdad AA, Morawska L, Mozaffarian D, Murphy T, Naghavi M, Neal B, Nelson PK, Nolla JM, Norman R, Olives C, Omer SB, Orchard J, Osborne R, Ostro B, Page A, Pandey KD, Parry CD, Passmore E, Patra J, Pearce N, Pelizzari PM, Petzold M, Phillips MR, Pope D, Pope CA 3rd, Powles J, Rao M, Razavi H, Rehfuess EA, Rehm JT, Ritz B, Rivara FP, Roberts T, Robinson C, Rodriguez-Portales JA, Romieu I, Room R, Rosenfeld LC, Roy A, Rushton L, Salomon JA, Sampson U, Sanchez-Riera L, Sanman E, Sapkota A, Seedat S, Shi P, Shield K, Shivakoti R, Singh GM, Sleet DA, Smith E, Smith KR, Stapelberg NJ, Steenland K, Stockl H, Stovner LJ, Straif K, Straney L, Thurston GD, Tran JH, Van Dingenen R, van Donkelaar A, Veerman JL, Vijayakumar L, Weintraub R, Weissman MM, White RA, Whiteford H, Wiersma ST, Wilkinson JD, Williams HC, Williams W, Wilson N, Woolf AD, Yip P, Zielinski JM, Lopez AD, Murray CJ, Ezzati M, AlMazroa MA and Memish ZA. A comparative risk assessment of burden of disease and injury attributable to 67 risk factors and risk factor clusters in 21 regions, 1990-2010: a systematic analysis for the Global Burden of Disease Study 2010. Lancet 2012; 380: 2224-2260.

[2] Schiffrin EL. Vascular remodeling in hypertension: mechanisms and treatment. Hypertension 2012; 59: 367-374.

[3] Suzuki R, Fukuda N, Katakawa M, Tsunemi A, Tahira Y, Matsumoto T, Ueno T and Soma M. Effects of an angiotensin II receptor blocker on the impaired function of endothelial progenitor cells in patients with essential hypertension. Am J Hypertens 2014; 27: 695-701.

[4] Yamamoto E, Kataoka K, Shintaku H, Yamashita T, Tokutomi Y, Dong YF, Matsuba S, Ichijo H, Ogawa H and Kim-Mitsuyama S. Novel mechanism and role of angiotensin II induced vascular endothelial injury in hypertensive diastolic heart failure. Arterioscler Thromb Vasc Biol 2007; 27: 2569-2575.

[5] Montezano AC, Nguyen Dinh Cat A, Rios FJ and Touyz RM. Angiotensin II and vascular injury. Curr Hypertens Rep 2014; 16: 431.

[6] De Ciuceis C, Amiri F, Brassard P, Endemann DH, Touyz RM and Schiffrin EL. Reduced vascular remodeling, endothelial dysfunction, and oxidative stress in resistance arteries of angiotensin II-infused macrophage colony-stimulating factor-deficient mice: evidence for a role in inflammation in angiotensin-induced vascular injury. Arterioscler Thromb Vasc Biol 2005; 25: 2106-2113.

[7] Barhoumi T, Kasal DA, Li MW, Shbat L, Laurant P, Neves MF, Paradis P and Schiffrin EL. T regulatory lymphocytes prevent angiotensin II-induced hypertension and vascular injury. Hypertension 2011; 57: 469-476.

[8] Suzuki Y, Ruiz-Ortega M, Lorenzo O, Ruperez M, Esteban V and Egido J. Inflammation and

angiotensin II. Int J Biochem Cell Biol 2003; 35: 881-900.
[9] Nagai N, Izumi-Nagai K, Oike Y, Koto T, Satofuka S, Ozawa Y, Yamashiro K, Inoue M, Tsubota K, Umezawa K and Ishida S. Suppression of diabetes-induced retinal inflammation by blocking the angiotensin II type 1 receptor or its downstream nuclear factor-kappaB pathway. Invest Ophthalmol Vis Sci 2007; 48: 4342-4350.
[10] Wang L, Hu X, Zhang W and Tian F. Angiotensin (1-7) ameliorates angiotensin II-induced inflammation by inhibiting LOX-1 expression. Inflamm Res 2013; 62: 219-228.
[11] Ijaz T, Sun H, Pinchuk IV, Milewicz DM, Tilton RG and Brasier AR. Deletion of NF-kappaB/RelA in angiotensin II-sensitive mesenchymal cells blocks aortic vascular inflammation and abdominal aortic aneurysm formation. Arterioscler Thromb Vasc Biol 2017; 37: 1881-1890.
[12] Hsu HH, Hoffmann S, Di Marco GS, Endlich N, Peter-Katalinic J, Weide T and Pavenstadt H. Downregulation of the antioxidant protein peroxiredoxin 2 contributes to angiotensin II-mediated podocyte apoptosis. Kidney Int 2011; 80: 959-969.
[13] Singh VP, Le B, Khode R, Baker KM and Kumar R. Intracellular angiotensin II production in diabetic rats is correlated with cardiomyocyte apoptosis, oxidative stress, and cardiac fibrosis. Diabetes 2008; 57: 3297-3306.
[14] Gonzalez A, Lopez B, Ravassa S, Querejeta R, Larman M, Diez J and Fortuno MA. Stimulation of cardiac apoptosis in essential hypertension: potential role of angiotensin II. Hypertension 2002; 39: 75-80.
[15] Zhang ZR, Leung WN, Cheung HY and Chan CW. Osthole: a review on its bioactivities, pharmacological properties, and potential as alternative medicine. Evid Based Complement Alternat Med 2015; 2015: 919616.
[16] You L, Feng S, An R and Wang X. Osthole: a promising lead compound for drug discovery from a traditional Chinese medicine (TCM). Nat Prod Commun 2009; 4: 297-302.
[17] Wang R, Kong J, Wang D, Lien LL and Lien EJ. A survey of Chinese herbal ingredients with liver protection activities. Chin Med 2007; 2: 5.
[18] Hoult JR and Paya M. Pharmacological and biochemical actions of simple coumarins: natural products with therapeutic potential. Gen Pharmacol 1996; 27: 713-722.
[19] Hua KF, Yang SM, Kao TY, Chang JM, Chen HL, Tsai YJ, Chen A, Yang SS, Chao LK and Ka SM. Osthole mitigates progressive IgA nephropathy by inhibiting reactive oxygen species generation and NF-kappaB/NLRP3 pathway. PLoS One 2013; 8: e77794.
[20] Yu C, Li P, Qi D, Wang L, Qu HL, Zhang YJ, Wang XK and Fan HY. Osthole protects sepsis-induced acute kidney injury via down-regulating NF-kappaB signal pathway. Oncotarget 2017; 8: 4796-4813.
[21] Wu SJ. Osthole attenuates inflammatory responses and regulates the expression of inflammatory mediators in HepG2 cells grown in differentiated medium from 3T3-L1 preadipocytes. J Med Food 2015; 18: 972-979.
[22] Chen Z, Mao X, Liu A, Gao X, Chen X, Ye M, Ye J, Liu P, Xu S, Liu J, He W, Lian Q and Pi R. Osthole, a natural coumarin improves cognitive impairments and BBB dysfunction after transient global brain ischemia in C57 BL/6J mice: involvement of Nrf2 pathway. Neurochem Res 2015; 40: 186-194.
[23] Ramos K and Cox LR. Primary cultures of rat aortic endothelial and smooth muscle cells: I. An in vitro model to study xenobiotic-induced vascular cytotoxicity. In Vitro Cell Dev Biol 1987; 23: 288-296.
[24] Deng B, Xie S, Wang J, Xia Z and Nie R. Inhibition of protein kinase C beta(2) prevents tumor necrosis factor-alpha-induced apoptosis and oxidative stress in endothelial cells: the role of NADPH oxidase subunits. J Vasc Res 2012; 49: 144-159.
[25] Morris GM, Huey R, Lindstrom W, Sanner MF, Belew RK, Goodsell DS and Olson AJ. AutoDock4 and AutoDockTools4: automated docking with selective receptor flexibility. J Comput Chem 2009; 30: 2785-2791.
[26] Jnoff E, Albrecht C, Barker JJ, Barker O, Beaumont E, Bromidge S, Brookfield F, Brooks M, Bubert C, Ceska T, Corden V, Dawson G, Duclos S, Fryatt T, Genicot C, Jigorel E, Kwong J, Maghames R, Mushi I, Pike R, Sands ZA, Smith MA, Stimson CC and Courade JP. Binding mode and structure-activity relationships around direct inhibitors of the Nrf2-Keap1 complex. ChemMedChem 2014; 9: 699-705.
[27] Chen YQ, Ghosh S and Ghosh G. A novel DNA recognition mode by the NF-kappa B p65 homodimer. Nat Struct Biol 1998; 5: 67-73.
[28] Marcotte D, Zeng W, Hus JC, McKenzie A, Hession C, Jin P, Bergeron C, Lugovskoy A, Enyedy I, Cuervo H, Wang D, Atmanene C, Roecklin D, Vecchi M, Vivat V, Kraemer J, Winkler D, Hong V, Chao J, Lukashev M and Silvian L. Small molecules inhibit the interaction of Nrf2 and the Keap1 Kelch domain through a non-covalent mechanism. Bioorg Med Chem 2013; 21: 4011-4019.
[29] Ramar V and Pappu S. Exploring the inhibitory potential of bioactive compound from Luffa acutangula against NF-kappaB-A molecular docking and dynamics approach. Comput Biol Chem 2016; 62: 29-35.

[30] Pang C, Zheng Z, Shi L, Sheng Y, Wei H, Wang Z and Ji L. Caffeic acid prevents acetaminophen-induced liver injury by activating the Keap1-Nrf2 antioxidative defense system. Free Radic Biol Med 2016; 91: 236-246.
[31] Wang J, Wolf RM, Caldwell JW, Kollman PA and Case DA. Development and testing of a general amber force field. J Comput Chem 2004; 25: 1157-1174.
[32] Lindorff-Larsen K, Piana S, Palmo K, Maragakis P, Klepeis JL, Dror RO and Shaw DE. Improved side-chain torsion potentials for the Amber ff99SB protein force field. Proteins 2010; 78: 1950-1958.
[33] Izaguirre JA, Catarello DP, Wozniak JM and Skeel RD. Langevin stabilization of molecular dynamics. J Chem Phys 2001; 114: 2090-2098.
[34] Essmann U, Perera L, Berkowitz ML, Darden T, Lee H and Pedersen LG. A smooth particle mesh Ewald method. J Chem Phys 1995; 103: 8577-8593.
[35] Kräutler V, Van Gunsteren WF and Hünenberger PH. A fast SHAKE algorithm to solve distance constraint equations for small molecules in molecular dynamics simulations. Journal of Computational Chemistry 2001; 22: 501-508.
[36] Miller BR 3rd, McGee TD Jr, Swails JM, Homeyer N, Gohlke H and Roitberg AE. MMPBSA.py: an efficient program for end-state free energy calculations. J Chem Theory Comput 2012; 8: 3314-3321.
[37] Onufriev A, Bashford D and Case DA. Exploring protein native states and large-scale conformational changes with a modified generalized born model. Proteins 2004; 55: 383-394.
[38] Hou T, Wang J, Li Y and Wang W. Assessing the performance of the MM/PBSA and MM/GBSA methods. 1. The accuracy of binding free energy calculations based on molecular dynamics simulations. J Chem Inf Model 2011; 51: 69-82.
[39] Cui J, Li Z, Zhuang S, Qi S, Li L, Zhou J, Zhang W and Zhao Y. Melatonin alleviates inflammation-induced apoptosis in human umbilical vein endothelial cells via suppression of Ca2+-XO-ROS-Drp1-mitochondrial fission axis by activation of AMPK/SERCA2a pathway. Cell Stress Chaperones 2018; 23: 281-293.
[40] Stan D, Calin M, Manduteanu I, Pirvulescu M, Gan AM, Butoi ED, Simion V and Simionescu M. High glucose induces enhanced expression of resistin in human U937 monocyte-like cell line by MAPK- and NF-kB-dependent mechanisms; the modulating effect of insulin. Cell Tissue Res 2011; 343: 379-387.
[41] Viatour P, Merville MP, Bours V and Chariot A. Phosphorylation of NF-kappaB and IkappaB proteins: implications in cancer and inflammation. Trends Biochem Sci 2005; 30: 43-52.
[42] Tang X, Yang X, Peng Y and Lin J. Protective effects of lycopene against H2O2-induced oxidative injury and apoptosis in human endothelial cells. Cardiovasc Drugs Ther 2009; 23: 439-448.
[43] Kotamraju S, Tampo Y, Keszler A, Chitambar CR, Joseph J, Haas AL and Kalyanaraman B. Nitric oxide inhibits H2O2-induced transferrin receptor-dependent apoptosis in endothelial cells: role of ubiquitin-proteasome pathway. Proc Natl Acad Sci U S A 2003; 100: 10653-10658.
[44] Lin H, Pan S, Meng L, Zhou C, Jiang C, Ji Z, Chi J and Guo H. MicroRNA-384-mediated Herpud1 upregulation promotes angiotensin II-induced endothelial cell apoptosis. Biochem Biophys Res Commun 2017; 488: 453-460.
[45] Lu Y, Wang RH, Guo BB and Jia YP. Quercetin inhibits angiotensin II induced apoptosis via mitochondrial pathway in human umbilical vein endothelial cells. Eur Rev Med Pharmacol Sci 2016; 20: 1609-1616.
[46] Savoia C, Burger D, Nishigaki N, Montezano A and Touyz RM. Angiotensin II and the vascular phenotype in hypertension. Expert Rev Mol Med 2011; 13: e11.
[47] Ndisang JF, Vannacci A and Rastogi S. Oxidative stress and inflammation in obesity, diabetes, hypertension, and related cardiometabolic complications. Oxid Med Cell Longev 2014; 2014: 506948.
[48] Fusi F, Sgaragli G, Ha le M, Cuong NM and Saponara S. Mechanism of osthole inhibition of vascular Ca(v)1.2 current. Eur J Pharmacol 2012; 680: 22-27.
[49] Akishita M, Nagai K, Xi H, Yu W, Sudoh N, Watanabe T, Ohara-Imaizumi M, Nagamatsu S, Kozaki K, Horiuchi M and Toba K. Renin-angiotensin system modulates oxidative stress-induced endothelial cell apoptosis in rats. Hypertension 2005; 45: 1188-1193.
[50] Rounds S, Farber HW, Hill NS and O'Brien RF. Effects of endothelial cell injury on pulmonary vascular reactivity. Chest 1985; 88: 213S-216S.
[51] Welch WJ. Angiotensin II-dependent superoxide: effects on hypertension and vascular dysfunction. Hypertension 2008; 52: 51-56.
[52] Marchesi C, Paradis P and Schiffrin EL. Role of the renin-angiotensin system in vascular inflammation. Trends Pharmacol Sci 2008; 29: 367-374.
[53] Ji Y, Liu J, Wang Z and Liu N. Angiotensin II induces inflammatory response partly via toll-like receptor 4-dependent signaling pathway in vascular smooth muscle cells. Cell Physiol Biochem 2009; 23: 265-276.
[54] Huang T and Dong Z. Osthole protects against inflammation in a rat model of chronic kidney

failure via suppression of nuclear factor-kappaB, transforming growth factor-beta1 and activation of phosphoinositide 3-kinase/protein kinase B/nuclear factor (erythroid-derived 2)-like 2 signaling. Mol Med Rep 2017; 16: 4915-4921.

[55] Ma Q. Role of nrf2 in oxidative stress and toxicity. Annu Rev Pharmacol Toxicol 2013; 53: 401-426.

[56] Li J, Zhang C, Xing Y, Janicki JS, Yamamoto M, Wang XL, Tang DQ and Cui T. Up-regulation of p27(kip1) contributes to Nrf2-mediated protection against angiotensin II-induced cardiac hypertrophy. Cardiovasc Res 2011; 90: 315-324.

[57] Ryter SW, Kim HP, Hoetzel A, Park JW, Nakahira K, Wang X and Choi AM. Mechanisms of cell death in oxidative stress. Antioxid Redox Signal 2007; 9: 49-89.

[58] Shokoohinia Y, Hosseinzadeh L, Moieni-Arya M, Mostafaie A and Mohammadi-Motlagh HR. Osthole attenuates doxorubicin-induced apoptosis in PC12 cells through inhibition of mitochondrial dysfunction and ROS production. Biomed Res Int 2014; 2014: 156848.

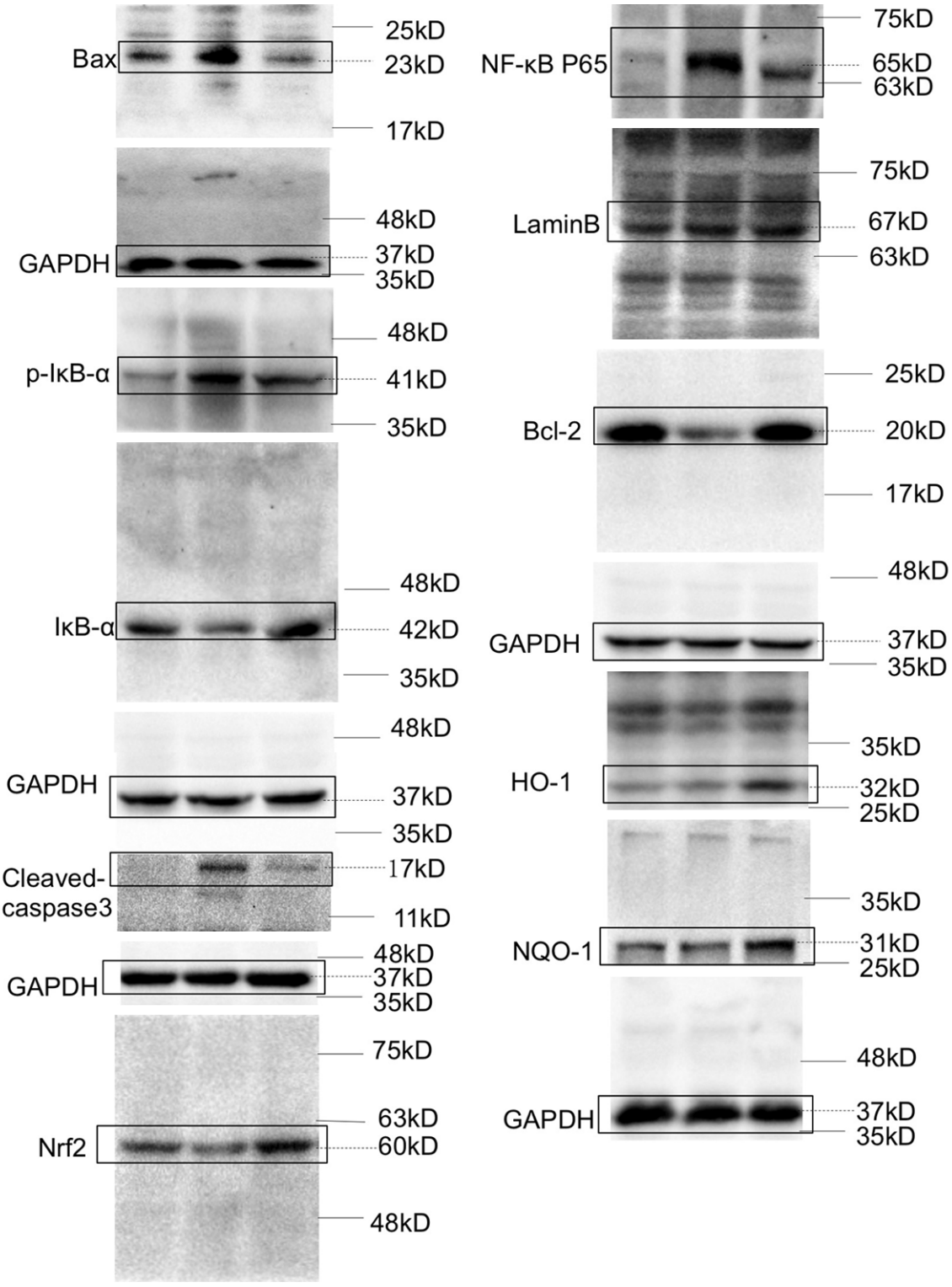


**Figure S1.** Original western images for all relevant western blots.